Conf-920308--11

To be Presented at The American Nuclear Society Meeting,
Advances in Reactor Physics, Charleston, SC March 8-11, 1992

An Improved Quasistatic Option for the DIF3D Nodal Kinetics Code

ANL/CP--73636

DE92 007376

T. A. Taiwo, and H. S. Khalil

Reactor Analysis Division
Argonne National Laboratory
9700 South Cass Avenue
Argonne, IL 60439
(708) 972-5621

* Work supported by the U.S. Department of Energy, Nuclear Energy Programs under Contract W-31-109-ENG-38.

AN IMPROVED QUASISTATIC OPTION FOR THE DIF3D NODAL KINETICS CODE

T. A. Taiwo and H. S. Khalil
Reactor Analysis Division
Argonne National Laboratory
Argonne, Illinois 60439, U.S.A.

ABSTRACT

An improved quasistatic scheme is formulated for solution of the time-dependent DIF3D nodal equations in hexagonal-z geometry. This scheme has been implemented, along with adiabatic and point kinetics solution options, in the DIF3D hexagonal-z nodal kinetics code. The improved quasistatic method is shown to permit significant reduction in computing time, even for transients involving pronounced changes in flux shape. The achievable computing time reduction, in addition to being problem dependent, has also been found to be larger when greater accuracy is required in the computed results.

INTRODUCTION

The formulation of an improved quasistatic scheme [1-3] and other space-time factorization schemes (adiabatic and point kinetics) for solution of the time-dependent DIF3D nodal diffusion equations in hexagonal-z geometry [4,5] is described. The objective of this formulation is to combine the computational efficiency and accuracy of the DIF3D nodal spatial differencing method with the potential efficiency advantage of the quasistatic approach for the analysis of transients in which the flux shape changes more slowly than its amplitude.

The quasistatic schemes have been implemented along with the theta-method described in reference 5 as a set of options in a time-dependent version of the DIF3D nodal code. This code can be executed either in a "stand-alone" mode with a specified time variation of the input cross sections or as a space-time neutronics module in a reactor dynamics code. The DIF3D nodal kinetics code has been successfully implemented, along with a correlation scheme for representing feedback effects on nodal cross sections, in the SAS-HWR dynamics code [6] being developed at ANL for the analysis of heavy-water reactor transients, including postulated severe accidents.

In this paper, we first derive the expressions for the kinetics parameters appearing in the (point) kinetics equations describing the variation of the flux amplitude; no approximations are introduced in deriving these equations, and their solution would reproduce the "exact" DIF3D nodal space-time results (e.g. obtained with the theta-method using very fine time steps) provided the actual time-dependent flux shape is used to compute the time-dependent kinetics parameters. We then discuss the approximations to the flux shape that distinguish the different space-time factorization options and describe the numerical solution techniques used to determine the flux shape in each case and to compute the flux amplitude. Finally, we compare the efficiency and accuracy of the various DIF3D

nodal space-time factorization options and of the theta method for two types of test problems in hexagonal-z geometry. For a 2-D (planar hexagonal) problem, we compare the DIF3D improved quasistatic solution to that obtained using the 2-D finite-difference code FX2-TH [2], which employs a somewhat different improved quasistatic solution scheme.

MATHEMATICAL FORMULATION

Time-Dependent Nodal Equations

The principal unknowns in the time-dependent DIF3D nodal equations [5] are the flux moments, partial currents, and the precursor concentration moments. The time-dependent equations for the flux moments and the partial currents can be cast into a supermatrix equation of the form

$$\begin{pmatrix} [v]^{-1} & [0] & [0] & [0] & [0] & [0] \\ [0] & [v]^{-1} & [0] & [0] & [0] & [0] \\ [0] & [0] & [v]^{-1} & [0] & [0] & [0] \\ [0] & [0] & [0] & [v]^{-1} & [0] & [0] \\ [0] & [0] & [0] & [0] & [v]^{-1} & [0] \\ [0] & [0] & [0] & [0] & [0] & [0] \end{pmatrix} \frac{d}{dt} \begin{pmatrix} \underline{\bar{\phi}} \\ \underline{\phi}_{x1} \\ \underline{\phi}_{u1} \\ \underline{\phi}_{v1} \\ \underline{\phi}_{z1} \\ \underline{J}^{out} \end{pmatrix} = \begin{pmatrix} [F_a] & [0] & [0] & [0] & [0] & -[\hat{\varepsilon}] \\ [0] & [F_m] & [0] & [0] & [0] & -[\hat{\zeta}_x] \\ [0] & [0] & [F_m] & [0] & [0] & -[\hat{\zeta}_u] \\ [0] & [0] & [0] & [F_m] & [0] & -[\hat{\zeta}_v] \\ [0] & [0] & [0] & [0] & [F_a] & -[\hat{\zeta}_z] \\ [\hat{B}] & [\hat{B}_x] & [\hat{B}_u] & [\hat{B}_v] & [\hat{B}_z] & -[H] \end{pmatrix} \begin{pmatrix} \underline{\bar{\phi}} \\ \underline{\phi}_{x1} \\ \underline{\phi}_{u1} \\ \underline{\phi}_{v1} \\ \underline{\phi}_{z1} \\ \underline{J}^{out} \end{pmatrix}$$

$$+ \sum_{i=1}^{I} \lambda_i \begin{pmatrix} (\underline{\chi}_i \bar{C}_i) \\ (\underline{\chi}_i C_{i,x1}) \\ (\underline{\chi}_i C_{i,u1}) \\ (\underline{\chi}_i C_{i,v1}) \\ (\underline{\chi}_i C_{i,z1}) \\ (0) \end{pmatrix} . \qquad (1)$$

Here $\underline{\bar{\phi}}$ is a GxK column vector containing the zeroth-moment (node-average) flux for all groups g=1,...,G and all nodes k=1,...,K . The GxK column vector $\underline{\phi}_{s1}$ contains for all groups and nodes the first moment of the flux, taken along coordinate direction s (s=x,u,v,z). The vector $\underline{J}^{out}$ is of length 8xGxK and contains the outgoing partial currents for all node-surfaces (8 in 3-D), all groups, and all nodes; the first 8G elements contain the partial currents for the first node. The vectors $(\underline{\chi}_i \bar{C}_i)$ and $(\underline{\chi}_i C_{i,s1})$ are of length GxK; they contain for all nodes the node-average precursor concentration $\bar{C}_i^k$ and the s-direction first-moment precursor concentration $C_{i,s1}^k$, respectively, each multiplied by the node volume V^k and by $\underline{\chi}_i$ (a column vector of length G that contains the energy spectrum of neutrons emitted from precursors in family i, i=1,...,I). The parameter λ_i is the decay constant for precursor family i, and I is the number of precursor families. The matrix $[v]^{-1}$ is of size GKxGK and contains the products of the nodal volumes and the inverse group velocities. The matrices $[F_a]$ and $[F_m]$ are defined as

$$[F_a] = -[\Sigma^r] + [\Sigma^s] + [M_p]$$

and

$$[F_m] = -[\Sigma^r] - [\Sigma^D] + [\Sigma^s] + [M_p],$$

where the GKxGK block-diagonal matrices $[\Sigma^r]$, $[\Sigma^s]$ and $[M_p]$ contain the products of the nodal volumes with the removal cross sections, inscattering cross sections, and production cross sections, respectively. The elements of the GKxGK block-diagonal matrix $[\Sigma^D]$, are proportional to the group diffusion coefficient and the nodal axial mesh spacing. The matrices $[\hat{B}]$, $[H]$, $[\hat{\varepsilon}]$, $[\hat{B}_s]$ and $[\zeta_s]$, (s=x,u,v,z) are coupling coefficient matrices: $[\hat{\varepsilon}]$ and $[\zeta_s]$, (s=x,u,v) are GKx8GK block-diagonal matrices, $[\zeta_z]$ is a GKx8GK block-tridiagonal matrix (as a result of the quadratic transverse leakage approximation in the axial direction), $[\hat{B}]$ and $[\hat{B}_s]$ are 8GKxGK block-diagonal matrices, and $[H]$ is of size 8GKx8GK. These coupling coefficient matrices depend only on the diffusion coefficients and nodal dimensions.

Note that Eq. (1) does not contain incoming partial currents as unknowns because they have been eliminated in favor of outgoing partial currents by the relation expressing the continuity of partial currents at nodal surfaces.

The time-dependent equations for the precursor concentration moments are also cast in supermatrix form as

$$\frac{d}{dt}\begin{pmatrix} (\underline{\chi}_i\overline{C}_i) \\ (\underline{\chi}_i C_{i,x1}) \\ (\underline{\chi}_i C_{i,u1}) \\ (\underline{\chi}_i C_{i,v1}) \\ (\underline{\chi}_i C_{i,z1}) \end{pmatrix} = \begin{pmatrix} [M_i] & [0] & [0] & [0] & [0] \\ [0] & [M_i] & [0] & [0] & [0] \\ [0] & [0] & [M_i] & [0] & [0] \\ [0] & [0] & [0] & [M_i] & [0] \\ [0] & [0] & [0] & [0] & [M_i] \end{pmatrix} \begin{pmatrix} \overline{\underline{\phi}} \\ \underline{\phi}_{x1} \\ \underline{\phi}_{u1} \\ \underline{\phi}_{v1} \\ \underline{\phi}_{z1} \end{pmatrix} - \lambda_i \begin{pmatrix} (\underline{\chi}_i\overline{C}_i) \\ (\underline{\chi}_i C_{i,x1}) \\ (\underline{\chi}_i C_{i,u1}) \\ (\underline{\chi}_i C_{i,v1}) \\ (\underline{\chi}_i C_{i,z1}) \end{pmatrix}, \quad i = 1,2, \ \ldots \ ,I \ , \tag{2}$$

where the elements of the GKxGK block-diagonal matrix $[M_i]$ depend on β_i (the fraction of neutrons appearing as delayed neutrons from the decay of precursor family i), χ_{gi} (the energy spectrum of delayed neutrons), the production cross section $\nu\Sigma_g^{f,k}$, and the nodal volume V^k .

Derivation of the Kinetics Equations

The supermatrix Eqs. (1) and (2) are the starting point for the derivation of the space-time factorized DIF3D nodal equations. The unknown vector of flux moments and partial currents appearing in Eq. (1) is expressed as the product of a normalized shape vector $\underline{S}$ and a global amplitude function T , i.e.,

$$\underline{\Psi} \equiv \begin{pmatrix} \overline{\underline{\phi}} \\ \underline{\phi}_{x1} \\ \underline{\phi}_{u1} \\ \underline{\phi}_{v1} \\ \underline{\phi}_{z1} \\ \underline{J}^{out} \end{pmatrix} = \underline{S}T = \begin{pmatrix} \underline{S}_0 \\ \underline{S}_{x1} \\ \underline{S}_{u1} \\ \underline{S}_{v1} \\ \underline{S}_{z1} \\ \underline{S}_I^{out} \end{pmatrix} T \ . \tag{3}$$

The amplitude function is defined as

$$T = \underline{\psi}^{\dagger T} \begin{pmatrix} [v]^{-1} & [0] & [0] & [0] & [0] & [0] \\ [0] & [v]^{-1} & [0] & [0] & [0] & [0] \\ [0] & [0] & [v]^{-1} & [0] & [0] & [0] \\ [0] & [0] & [0] & [v]^{-1} & [0] & [0] \\ [0] & [0] & [0] & [0] & [v]^{-1} & [0] \\ [0] & [0] & [0] & [0] & [0] & [0] \end{pmatrix} \underline{\psi} = \overline{\phi}^{\dagger T}[v]^{-1}\overline{\phi} + \sum_{s=x,u,v,z} \underline{\phi}_{s1}^{\dagger T}[v]^{-1}\underline{\phi}_{s1} , \tag{4}$$

where $\underline{\psi}^{\dagger}$ is the initial state adjoint vector, defined as

$$\underline{\psi}^{\dagger} = \text{col}\,(\overline{\varphi}^{\dagger} , \underline{\phi}_{x1}^{\dagger} , \underline{\phi}_{u1}^{\dagger} , \underline{\phi}_{v1}^{\dagger} , \underline{\phi}_{z1}^{\dagger} , \overline{J}^{out\dagger}) ,$$

and $\underline{\psi}^{\dagger T}$ is its transpose. The initial state adjoint vector is computed using the mathematical nodal adjoint scheme in DIF3D [7].

If Eq. (3) is used to eliminate the vector of fluxes and partial currents, $\underline{\psi}$, from Eq. (4), we obtain the following normalization constraint on the shape vector

$$\overline{\phi}^{\dagger T}[v]^{-1}\underline{S}_0 + \sum_{s=x,u,v,z} \underline{\phi}_{s1}^{\dagger T}[v]^{-1}\underline{S}_{s1} = 1 . \tag{5}$$

For convenience, we define two vectors $\underline{S}_\phi$ and $\underline{\psi}_\phi^{\dagger}$ as follows:

$$\underline{S}_\phi = \text{col}\,(\underline{S}_0 , \underline{S}_{x1} , \underline{S}_{u1} , \underline{S}_{v1} , \underline{S}_{z1}) ,$$

and

$$\underline{\psi}_\phi^{\dagger} = \text{col}\,(\overline{\varphi}^{\dagger} , \underline{\phi}_{x1}^{\dagger} , \underline{\phi}_{u1}^{\dagger} , \underline{\phi}_{v1}^{\dagger} , \underline{\phi}_{z1}^{\dagger}) .$$

These vectors differ from $\underline{S}$ and $\underline{\psi}^{\dagger}$, respectively, only in the absence of the outgoing partial current components. We also define a block-diagonal supermatrix [M] which has the matrix $[M_p] + \sum_{i=1}^{I}[M_i]$ as its diagonal blocks. Premultiplying Eq. (1) by $\underline{\psi}^{\dagger T}$ and Eq. (2) by $\underline{\psi}_\phi^{\dagger}$, dividing the resulting equations by $\underline{\psi}_\phi^{\dagger T}[M]\underline{S}_\phi$, and using the definitions

$$\Lambda \equiv \frac{\overline{\phi}^{\dagger T}[v]^{-1}\underline{S}_0 + \sum_{s=x,u,v,z} \underline{\phi}_{s1}^{\dagger T}[v]^{-1}\underline{S}_{s1}}{\underline{\psi}_\phi^{\dagger T}[M]\underline{S}_\phi} , \tag{6}$$

$$\beta_{e,i} \equiv \frac{\underline{\bar{\phi}}^{*T}[M_i]\underline{S}_0 + \sum_{s=X,U,V,Z} \underline{\phi}_{s1}^{*T}[M_i]\underline{S}_{s1}}{\underline{\psi}_0^{*T}[M]\underline{S}_0} , \tag{7}$$

$$\beta_e = \sum_{i=1}^{I} \beta_{e,i} , \tag{8}$$

$$\begin{aligned}\rho \equiv \frac{1}{\underline{\psi}_0^{*T}[M]\underline{S}_0} \Bigg\{ & \underline{\bar{\phi}}^{*T}\left[\left([F_a] + \sum_{i=1}^{I}[M_i]\right)\underline{S}_0 - [\hat{\varepsilon}]\,\underline{S}_j^{out}\right] \\ & + \sum_{s=X,U,V} \underline{\phi}_{s1}^{*T}\left[\left([F_m] + \sum_{i=1}^{I}[M_i]\right)\underline{S}_{s1} - [\hat{\zeta}_s]\,\underline{S}_j^{out}\right] + \underline{\phi}_{z1}^{*T}\left[\left([F_a] + \sum_{i=1}^{I}[M_i]\right)\underline{S}_{z1} - [\hat{\zeta}_z]\,\underline{S}_j^{out}\right] \\ & + \underline{\bar{J}}^{out*T}\left([\hat{B}]\,\underline{S}_0 + \sum_{s=X,U,V,Z}[\hat{B}_s]\,\underline{S}_s - [H]\,\underline{S}_j^{out}\right)\Bigg\} ,\end{aligned} \tag{9}$$

and

$$C_i = \frac{\underline{\bar{\phi}}^{*T}(\underline{\chi}\overline{C}_i) + \sum_{s=X,U,V,Z} \underline{\phi}_{s1}^{*T}(\underline{\chi}\overline{C}_{i,s1})}{\underline{\bar{\phi}}^{*T}[v]^{-1}\underline{S}_0 + \sum_{s=X,U,V,Z} \underline{\phi}_{s1}^{*T}[v]^{-1}\underline{S}_{s1}} , \tag{10}$$

we obtain the conventional form of the kinetics equations, i.e.,

$$\frac{d}{dt}T = \frac{(\rho - \beta_e)}{\Lambda}T + \sum_{i=1}^{I}\lambda_i C_i \tag{11}$$

and

$$\frac{d}{dt}C_i = \frac{\beta_{e,i}}{\Lambda}T - \lambda_i C_i , \qquad i = 1,\ldots, I. \tag{12}$$

The parameters in these equations have the conventional meaning, i.e. Λ is the prompt neutron lifetime, $\beta_{e,i}$ is the effective delayed neutron fraction for family i, ρ is the reactivity, and C_i is the adjoint weighted precursor concentration for family i.

The kinetics equations, Eqs. (11) and (12), are common to all the factorization options and are solved simultaneously for the time variation of the flux amplitude T once the kinetics parameters have been determined. We note that no approximations are made in the derivation of these equations from the time-dependent nodal equations, and that it is the use of approximate shape vectors in

place of the exact time-dependent shape function that leads to deviations from exact space-time results (e.g. by utilizing the initial shape throughout a transient as in the conventional point kinetics model).

Approximation of the Time-Dependent Shape Vector

An approximation to the time-dependent shape vector is required to compute the kinetics parameters in Eqs. (6) to (9), as well as to obtain the time-dependent flux and power distributions once the amplitude function has been determined by solution of the kinetics equations. The accuracy of the solution depends on the accuracy of the shape vector used to compute the kinetics parameters, especially the reactivity.

In implementing the improved quasistatic scheme, we have opted to approximate the flux shape by solving the time-dependent DIF3D nodal equations [5] using the implicit scheme ($\theta = 1$) with large time-step sizes. It was shown by Kao and Henry [8] that the use of large time-steps for determining the shape vector provides sufficiently accurate results, even though the associated flux amplitude is quite inaccurate. (We have verified the accuracy of this approximate way of determining the shape function. Note that the exact shape results when a sufficiently small time-step size is used for the shape calculation.) The computed shape is normalized by application of the constraint provided by Eq. (5). This approach for determining the shape differs from that originally used by Ott and Meneley wherein an equation derived expressly for the shape vector $\underline{S}$ (as opposed to the equation for the flux, i.e. the product of the shape and amplitude), is solved with the large time-step.

In the adiabatic scheme, the shape is approximated by solving the time-independent DIF3D nodal equations at various instants during the transient, with the time-dependent nodal parameters taking on instantaneous values appropriate to the time at which the calculations are performed. Finally, in the point kinetics scheme, the initial shape vector is used to approximate the time-dependent shape for the entire transient duration.

SOLUTION TECHNIQUE

Three types of time intervals are defined in implementing the space-time factorization schemes. In decreasing order of time-step size, they are the shape step, the reactivity step, and the kinetics solution step; the smaller intervals are nested within the next larger interval. Another time interval, called a time domain, is also defined independently to facilitate the integration of the DIF3D nodal kinetics code in an integrated dynamics code such as SAS-HWR [6]. A time domain corresponds to the main thermal-hydraulic (T-H) step of the dynamics code, and T-H parameters which are calculated at the end of the main T-H step are used to compute new cross sections for the DIF3D kinetics calculation. Furthermore, the power densities are editted at the end of a time-domain, which typically consists of one or more reactivity steps. On the other hand, a shape interval can span more than one time domain.

The DIF3D nodal kinetics code internally computes the the kinetics, reactivity, and shape time-step sizes based on user-specified criteria. The time-step selection criteria are similar to those used in the FX2-TH code [2] and thus take advantage of previously developed modeling judgements. Across each kinetics step within a reactivity interval, the kinetics equations are solved with the modified Kaganove scheme [9,10], using linear or quadratic fits of the kinetics parameters determined at the beginning and end of each reactivity step. The solution of the kinetics equation progresses until the end of a reactivity step. The Kaganove scheme employs an automatic time-step halving and doubling algorithm to compute the time-step size needed to achieve a user-specified precision.

At the end of each reactivity step within a shape interval, new cross sections are calculated by linear interpolation of cross section data evaluated at bracketing time domain endpoints, and they are used along with the appropriate shape vector to compute the kinetics parameters ρ , $\beta_{e,i}$, and Λ . At a reactivity step endpoint within a shape interval (not corresponding to the endpoint of the shape interval), shape vectors required to compute the power distribution or kinetics parameters are obtained by linear extrapolation of the two preceding shape vectors. This extrapolation scheme can lead to inaccurate reactivity values if the rate of shape variation changes significantly prior to a shape recalculation (i.e. if the specified shape recalculation criteria are inadequate). The extrapolation scheme can optionally be disabled, in which case the shape step is the same as the reactivity step. At the end of each reactivity step, the shape vector is normalized and combined with the amplitude function (at the endpoint) to determine the flux vector and compute the power densities.

The size of a reactivity time-step is determined at the end of the preceding reactivity interval. To determine this reactivity time-step size, three time-step lengths are computed based on user-specified parameters and certain code constraints, and the minimum of these lengths is selected as the reactivity time-step size. The three time-step lengths are

1. An input maximum reactivity step length.

2. Twice the previous reactivity step length.

3. The reactivity step size for which the estimated amplitude function change, based on quadratic projection of the amplitude function, equals a user-specified maximum value.

The smallest of these time-step lengths is used as the reactivity step size only if it does not contain the endpoint of a time domain, the endpoint of a shape calculation, or the problem end-time. If the smallest time-step contains one of these end-times, the time-step size is adjusted so that the smallest of these times becomes the endpoint of the next reactivity step.

A shape calculation is performed at the end of a shape interval or at the end of an imbedded reactivity step (within the shape interval) if the shape recalculation criteria are met at that point. The fully-implicit option of the theta solution scheme [5] is used to compute the new shape vector. Since a shape interval endpoint also corresponds to the endpoint of the last imbedded reactivity step, kinetics parameters are obtained at this time point with the new shape vector, and the solution of the kinetics equations over this last reactivity step is obtained. The normalized shape vector and the amplitude function (at this endpoint) are then combined and used to obtain the flux and power density distributions. This new flux distribution is used along with information known at the end of the preceding shape interval to compute the precursor concentration moments.

The length of a shape interval is calculated at the end of the preceding shape interval. In order to determine the shape interval duration, three time-step lengths are computed based on user-specified parameters and code constraints, and the minimum of these lengths is selected as the shape interval. The three time-step lengths are

1. An input maximum shape step interval.

2. Ten times the previous shape interval.

3. The shape step size for which shape change estimated by linear extrapolation equals a user-specified maximum allowable shape change.

The smallest of these time-step lengths is used as the next shape interval size only if it does not contain the transient problem end-time. If it does, the time-step size is adjusted so that the problem end-time becomes the endpoint of the shape interval. A shape calculation is also enabled at the end of a reactivity step (within the shape interval) if the amplitude change thus far over the shape interval does not satisfy a user-specified value. The sizes of the very first reactivity step and shape interval are taken to be the same and are specified by the user as a multiple of the prompt neutron lifetime Λ.

NUMERICAL TEST RESULTS

Several test problems have been solved to verify the implementation of the various factorization schemes. Results of these problems confirmed that with very small shape time-step sizes, the improved quasistatic scheme reproduces the theta method results. As expected, substantial savings in computational time were achieved with the factorization options for problems involving minor shape changes.

Results are presented here for two numerical test cases with pronounced space-time effects. In each case, the initial core state is a hexagonal-z representation of a heavy-water reactor core [5,11]. The first case models the insertion of \$2.7 of (static) reactivity over 0.4 s through the reduction of the thermal capture cross section in the central core patch (central and six surrounding hexagonal cells) by a factor of 1.96. Table 1(a) compares the time evolution of the core power predicted by the improved quasistatic, adiabatic, and point kinetics schemes to the reference results obtained using the fully implicit scheme. The point kinetics scheme is seen to be extremely inaccurate for this transient involving a pronounced shape change. The adiabatic scheme is also inaccurate because asymptotic shapes are used to approximate the time-dependent shapes (which are not asymptotic in the time period of interest). For example, the adiabatic scheme predicts that the asymptotic reactivity is prematurely reached at 0.4 s; the reference (dynamic) reactivity is 2 % lower than the asymptotic reactivity at this time point. The asymptotic reactivity is reached by the reference solution only after 0.5 s has elapsed. On the other hand, the improved quasistatic scheme retains the accuracy of the reference solution, while requiring a factor of 8 less computing time. It should be noted however that the computing times given in Table 1 can be reduced at the expense of accuracy for both the quasistatic method (by relaxing shape recalculation criteria) and the fully implicit method (by increasing time step sizes). The savings in computing time achievable with the improved quasistatic scheme has been found to depend on the accuracy relative to the reference theta-method solution, as shown in Fig.1, which compares the computation time as a function of accuracy for the improved quasistatic (IQS) and theta schemes. It can be seen that the ratio of the computation time for the theta scheme to that for the improve quasistatic scheme decreases as the error in core power increases. This suggests that the theta method becomes more competitive as the accuracy requirement is relaxed.

The second problem simulates a delayed supercritical transient terminated by the insertion of negative reactivity. This transient was modelled by first linearly reducing the thermal capture cross section in the central patch by 28 % over the first 1.0 s, followed by an increase to 0.995 of the initial state value at 2.5 s. A reduction of the neutron yield per fission (ν) by 0.8 % was superimposed from 1.0 s to 3.0 s. The resulting reference reactivities, obtained with a fully implicit reference calculation, are presented in Table 1(b). This Table also compares the core power results provided by the improved quasistatic, adiabatic, and point kinetics options with the reference results. Again, the point kinetics scheme is very inaccurate, underpredicting the maximum core power by 40.6 %. The adiabatic scheme appears to be quite accurate for this problem even though it overpredicts the reactivity and the flux amplitude as a function of time (note that the calculated power additionally depends on the shape and benefits in this case from the compensation of the shape and amplitude errors). The improved quasistatic solution is very accurate and requires a factor of 13 less computing time than the reference solution. If an error of about 1.5 % in the core power is tolerable, the computation efficiency advantage of the improved quasistatic method is reduced to a factor of about 2.

As previously discussed, the DIF3D nodal quasistatic scheme obtains the time-dependent flux shape using the approach of reference 8, i.e. by solving the fully implicit DIF3D nodal equations with a large time step size. The alternative and more conventional approach is to solve an equation specifically derived for the shape, as is done for example in the 2-D finite-difference code FX2-TH [2]. To evaluate the implication of this difference in shape calculation approach on the required shape recalculation frequency, comparisons were made between DIF3D and FX2-TH improved quasistatic solutions for the 2-D (planar hexagonal) HWR problem referred to as test-case 2 in reference 5; in that problem, a reactivity increase of 75 cents was introduced over 0.2 s by reducing the absorption cross section in the central part of the core. The FX-2 solution was obtained using 24 triangular mesh cells per hexagon and employed the code default parameters [2] for controlling the duration of shape and reactivity intervals. The DIF3D improved quasistatic solution was obtained using essentially the same criteria for control of time step sizes. (In reference 5, the accuracy of the DIF3D nodal spatial differencing scheme was shown to be comparable to the 24 triangular mesh cells per hexagon finite difference scheme.) As shown in Table 2, the two codes yield quasistatic results of comparable accuracy and perform a similar total number of shape calculations, as well as a similar number of shape calculations during each of three portions of the total problem time. This result indicates that the DIF3D approach for obtaining the time-dependent shape does not adversely affect the accuracy of the computed results for a given shape recalculation frequency. Thus the substantially greater efficiency of the DIF3D nodal spatial differencing approach relative to the finite-difference approach is preserved in the DIF3D nodal quasistatic solution of time-dependent problems.

SUMMARY AND CONCLUSIONS

The formulation of three different space-time factorization options for solution of the time-dependent DIF3D nodal diffusion equations in hexagonal-z geometry has been presented. These options (point kinetics, adiabatic, and improved quasistatic) have been implemented, along with the existing theta time integration scheme, in the DIF3D nodal kinetics code. The availability of all options in one code provides substantial flexibility for minimizing the computational cost of analyzing different types of transients.

The space-time factorization options performed, as expected, substantially better than the theta method for problems with relatively mild variations in the flux shape. However, even for problems with pronounced space-time effects, the improved quasistatic method outperformed the fully implicit method.

The computing efficiency advantage of the improved quasistatic method over the fully implicit method, in addition to being problem dependent, has also been found to depend on the (common) accuracy requirement imposed on the two solutions, as controlled by the respective time step sizes. In particular, the efficiency advantage of the improved quasistatic method appears to be greater when higher accuracy in computed power is required. More definitive conclusions about the comparative performance of the different transient solution options will become available in the context of analyzing specific transients using the integrated SAS-HWR/DIF3D-nodal dynamics code currently being developed at ANL.

REFERENCES

1. K. O. Ott and D. A. Meneley, "Accuracy of the Quasistatic Treatment of Spatial Reactor Kinetics," Nucl. Sci. Eng., 36, p. 402, 1969.

2. R. A. Shober, T. A. Daly, and D. R. Ferguson, "FX2-TH: A Two-Dimensional Nuclear Reactor Kinetics Code With Thermal-Hydraulic Feedback," ANL-78-97, Argonne National Laboratory, October 1978.

3. H. L. Dodds, Jr., "Accuracy of the Quasistatic Method for Two-Dimensional Thermal Reactor Transients With Feedback," Nucl. Sci. Eng., 59, p. 271, 1976.

4. R. D. Lawrence, "The DIF3D Nodal Neutronics Option for Two- and Three-Dimensional Diffusion Theory Calculations in Hexagonal Geometry," ANL-83-1, Argonne National Laboratory, March 1983.

5. T. A. Taiwo and H. S. Khalil, "The DIF3D Nodal Kinetics Capability in Hexagonal-Z Geometry -- Formulation and Preliminary Tests," Proceedings of the International Topical Meeting on Advances in Mathematics, Computations, and Reactor Physics, Pittsburgh, Pennsylvania, p. 23.2 2-1, American Nuclear Society, April 1991.

6. E. E. Morris, ANL, Private Communication, October 1990.

7. R. D. Lawrence, "Perturbation Theory Within the Framework of a Higher Order Nodal Method," Trans. Am. Nucl. Soc., 46, 402 (1984).

8. P. Kao and A. F. Henry, "Supernodal Analysis of PWR Transients," Proceedings of the Topical Meeting on Advances in Nuclear Engineering Computation and Radiation Shielding, Santa Fe, New Mexico, p. 63, Vol. 2, American Nuclear Society, April 1989.

9. J. J. Kaganove, "Numerical Solution of the One-Group Space-Independent Reactor Kinetics Equations for Neutron Density Given Excess Reactivity," ANL-6132, Argonne National Laboratory (1960).

10. E. L. Fuller, "The Point Kinetics Algorithm for FX2," ANL-7910, Argonne National Laboratory, p. 503, 1976.

11. M. R. Buckner and J. W. Stewart, "Multidimensional Space-Time Nuclear-Reactor Kinetics Studies-Part I: Theoretical," Nucl. Sci. Eng., 59, p. 289, 1976.

Table 1(a): Test Case 1 Results

Time (s)	Reference Reactivity[a]	CORE POWER				
		Theta[a]	Improved Quasistatic[b]	Improved Quasistatic[c]	Point Kinetics	Adiabatic[c]
0.00	0.00000	1.0000	1.0000	1.0000	1.0000	1.0000
0.10	0.00908	1.8251	1.8247	1.8256	1.4801	1.8793
0.20	0.01177	8.9447	8.9415	8.9558	2.3334	9.8805
0.30	0.01428	60.295	60.289	60.615	3.1238	70.024
0.40	0.01715	801.63	801.87	810.56	4.0502	999.39
0.50	0.01726	16669.	16658.	16981.	5.0256	21918.
No. of shape calcs.		-	303	78	-	78
No. of time steps		11076	308	85	9	84
Computation time, s[d]		3616	462	177	23	288

Table 1(b): Test Case 2 Results

Time (s)	Reference Reactivity[a]	CORE POWER			
		Theta[a]	Improved Quasistatic[c]	Point Kinetics	Adiabatic[c]
0.00	0.00000	1.0000	1.0000	1.0000	1.0000
0.10	0.00034	1.0261	1.0261	1.0279	1.0253
0.20	0.00071	1.0782	1.0784	1.0788	1.0774
0.50	0.00207	1.3427	1.3432	1.2851	1.3451
1.00	0.00557	3.1814	3.1831	1.8911	3.2612
1.50	0.00104	1.5448	1.5460	1.2253	1.5615
2.00	-.00275	0.8245	0.8247	0.7527	0.8283
2.50	-.00608	0.5919	0.5921	0.5489	0.5957
3.00	-.00814	0.4926	0.4927	0.4561	0.4958
No. of shape calcs.		-	49	-	52
No. of time steps		4549	58	12	61
Computation time, s[d]		1734	133	28	170

[a] Reference solution computed with fully implicit option employing variable time-step size ($\omega\Delta t=10^{-3}$, where ω is the inverse of the local period and Δt is the time-step size).

[b] Shape recalculation based on 2.5 % maximum local shape change.

[c] Shape recalculation based on 10% maximum shape change.

[d] On the ANL Cray X-MP/18 computer.

Table 2: Comparison of FX2-TH and DIF3D Improved Quasistatic Solutions

Time (s)	DIF3D Fully Implicit[a]		DIF3D-Improved Quasistatic[b]		FX2-TH[b]	
	Core Power	Reactivity	Core Power	Reactivity	Core Power	Reactivity
0.00	1.0000	0.00000	1.0000	0.00000	1.0000	0.00000
0.01	1.0077	0.00019	1.0068	0.00019	1.0071	0.00019
0.05	1.0991	0.00099	1.0979	0.00099	1.0999	0.00099
0.20	2.4213	0.00527	2.4108	0.00527	2.3990	0.00524
0.50	4.9110	0.00533	4.9425	0.00533	4.8568	0.00531
1.00	7.4772	0.00534	7.4992	0.00534	7.3520	0.00532
1.50	10.862	0.00535	10.890	0.00535	10.626	0.00533
2.00	15.514	0.00535	15.553	0.00535	15.099	0.00533
2.50	21.975	0.00536	22.030	0.00536	21.277	0.00534
3.00	30.986	0.00536	31.063	0.00536	29.843	0.00534
Λ (s) at 0.0 s	1.4865E-04		1.4864E-04		1.4855E-04	
Λ (s) at 3.0 s	1.4685E-04		1.4685E-04		1.4682E-04	
β_e at 3.0 s	7.1804E-03		7.1804E-03		7.1804E-03	
No. of Shape Calc. in 0.0 - 0.2 s			10		14	
No. of Shape Calc. in 0.2 - 0.5 s			3		4	
No. of Shape Calc. in 0.5 - 3.0 s			13		14	
Total No. of Shape Calc.			26		32	
CPU (s)	111.06[c]		7.22[c]		602.84[d]	

[a] Reference nodal solution computed with time step size Δt=0.0025 s

[b] Improved quasistatic cases employ the default time step selection criteria in FX2-TH [2].

[c] On the ANL Cray X-MP/18 Computer.

[d] On the ANL IBM-3084 Computer.

Fig. 1: Computation Time Versus Maximum Error

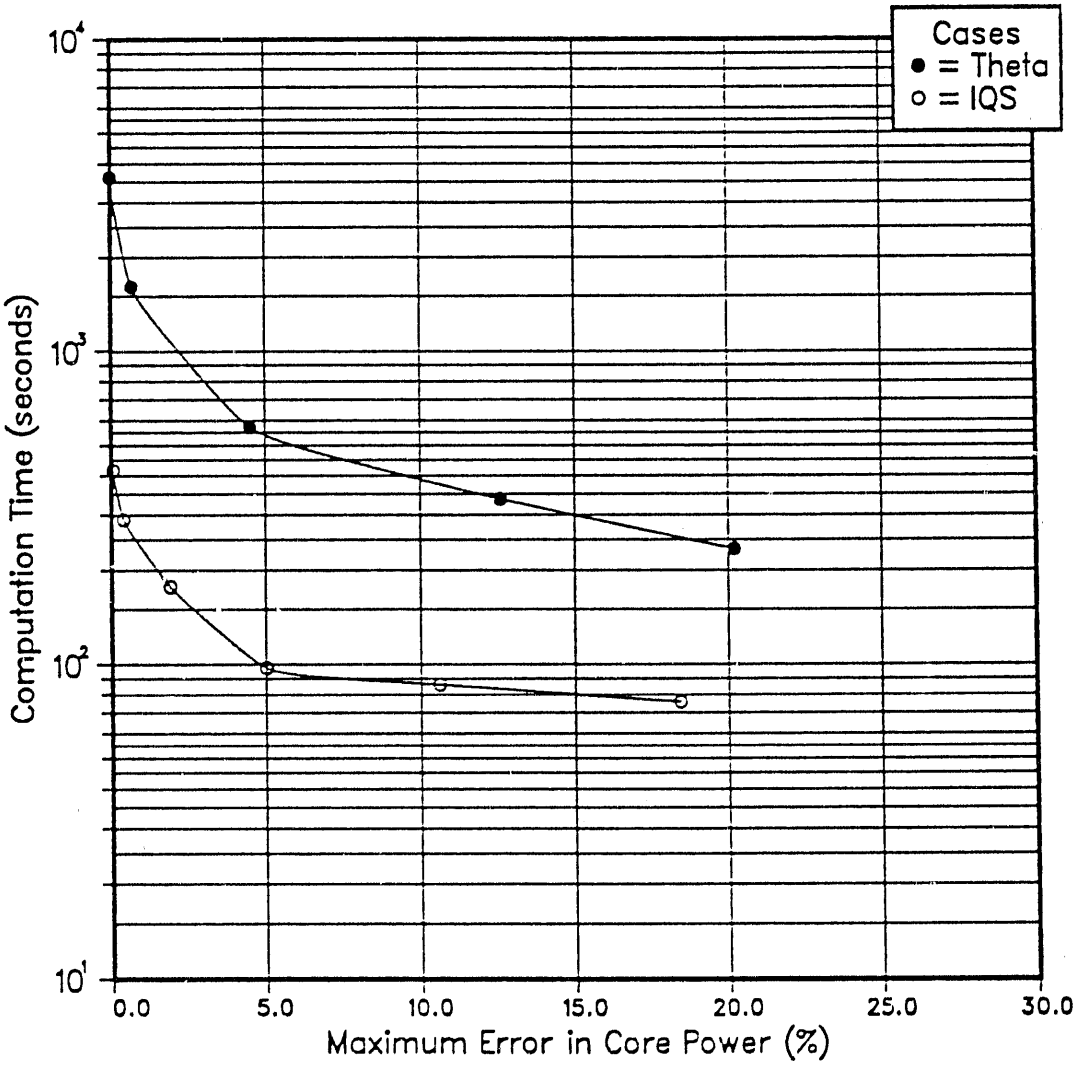

END

DATE FILMED

3/9/92